Journal of Visualization, Vol. 8, No. 4 (2005)305-313

Visualization of a Wall Shear Flow

Development of a New Particle Image Interrogation Method

Debaene, P.*, Kertzscher, U.*, Goubergrits, L.* and Affeld, K.*

* Biofluidmechanics Laboratory, Charité Universitätsmedizin Berlin, Spandauer Damm 130, 14050 Berlin, Germany. E-mail: perrine.debaene@charite.de

Received 29 October 2004
Revised 5 May 2005

Abstract : In this paper we propose a new method which might be useful to investigate the flow fields close to vaulted walls with spatial and temporal resolution. This kind of flow visualization is important in the field of biofluid mechanics, since a close relationship is assumed between flow and biological phenomena. This new method is non-invasive, and is also applicable for unsteady flows. It has been used to investigate the steady and the unsteady laminar flow in a rectangular duct, as well as the steady, laminar flow in two different U-shaped ducts, both with a backward facing step, one having a rectangular cross-section, the other a nearly elliptical cross-section. The results concurred well with analytical or numerical solutions.

Keywords : Velocity measurement, Wall shear stress, Biofluid mechanics.

1. Introduction

The investigation of the flow near the wall of a blood vessel or an artificial organ is of great interest, since it is known that there is a close relationship between flow and biological phenomena like thrombus formation (Morton and Cumming, 1977) or atherosclerotic events (Asakura and Karino, 1990). In particular, the wall shear stress plays a role because it influences the structure and function of the endothelial cells (Nerem et al., 1998) as well as the behavior of platelets (Kroll et al., 1996). The flow and the reaction of the vessel wall or the artificial surface are well connected (Asztalos et al., 2000). However, quantification is still lacking. Numerous factors influence the interaction and make a correlation between wall shear stress and wall alterations difficult.

The measurement of the flow close to the wall, especially of the wall shear stress, is a precondition to our understanding of atherosclerotic events and also our ability to avoid thrombus generation in artificial organs. Nevertheless it remains a challenging experimental problem. Reasons for this are the pulsatile flow, the vaulted and moving walls, and, depending on the model, the small diameter. There is no adequate technique for a time-resolved investigation of the whole flow close to a vaulted wall. Laser Doppler Velocimetry (LDV) has a high resolution and is very precise, but it is a single point measurement. Conventional, multi-slice, or stereoscopic Particle Image Velocimetry (PIV) also proves inadequate since PIV is based on a planar illumination. Holographic PIV still requires an enormous computing and analysis time. 3D Particle Tracking has a limited spatial resolution because of the low particle image density.

The method we propose here has the potential to solve the aforementioned dilemma.

2. Method

Our new method is based on the observation and digital recording of small, buoyant, light reflecting particles suspended in the fluid. Hence it is a particle image interrogation method. The transparent flow model is illuminated from the outside with monochromatic diffuse light. A dye is added to the fluid, which limits the penetration depth of the light into the flow model. According to optical laws, the penetration depth decreases if the concentration of the dye increases. Thus, the whole flow near the wall is illuminated and all the particles located near the wall become visible. Within the illuminated layer, the particles appear more or less bright, depending on their distance from the wall, d_p. Particles near the wall appear brighter, i.e., have a higher gray value, than particles farther from the wall (see Fig. 1).

An image processing leads to a separation of the near-wall flow in several layers. All the particles moving in one layer have the same gray value and, therefore, the same distance from the wall, d_p. For each layer, the motion of the particles can be determined with a conventional PIV algorithm. It results in a vector field for each layer. In case of vaulted walls velocity values have to be corrected to take the three-dimensionality into account. If the concentration of the dye, the lighting and the size of the particles are properly chosen, the particles closest to the wall are within the region where the velocity distribution is considered as proportional to the wall distance. For a Newtonian fluid, this allows the calculation of wall shear stress, $\tau_{w,}$ by using the measured velocity component parallel to the wall, v_p, the distance from the wall, d_p, and the dynamic viscosity of the fluid, η, by Eq. (1):

$$\tau_w = \eta \frac{v_p}{d_p} \tag{1}$$

If the particles undergo a non-linear velocity gradient, the velocity at the center of a particle is not the average velocity of both velocities at the opposite sides of the sphere. It is impossible to know which velocity is going to be measured, and thus to produce reliable results.

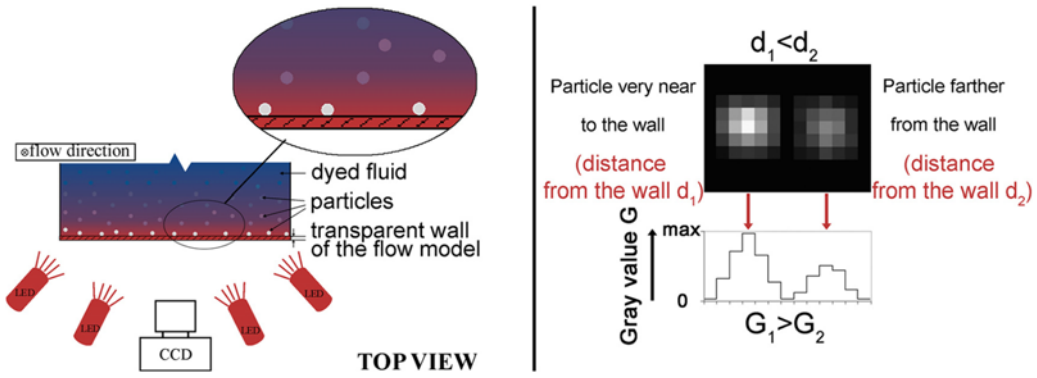

Fig. 1. Left: Basic idea of the new method for the visualization of the flow close to the wall. Right, top: two particles with the same diameter but different distances from the wall and therefore different gray values. Right, bottom: Gray value profile along the middle line of the picture on the top.

2.1 Experimental Parameters

The particles have to be neutrally buoyant. They should not alter the flow and should not interact with each other. They should be spherical and monodisperse, otherwise it is impossible to process a valuable separation of the illuminated layer. Furthermore, the particles should reflect the light as efficiently as possible. Special particles were developed to fulfill these requirements. Encapsulated alginatbeads with glass hollow micro-spheres were manufactured by LUM GmbH (Berlin, Germany) using the vibrating nozzle technique. The encapsulation device is based on the break-up of a laminar jet induced by applying a sinusoidal frequency with defined amplitude to the nozzle. It allows obtaining small particles with a narrow size distribution. The glass micro-spheres permit a density

fitting of the beads. The particles we used have a mean diameter of d = 350 or 360 μm, with a standard deviation smaller than 3% (Heinzen, 1996) by a density of ca. 1.1 $g \cdot cm^{-3}$. We assume the particles follow the flow, even in the wall vicinity. This assumption will be addressed in Sec. 4.

We made use of a high-speed video camera (Fastcam Super 10 K, Roper Scientific MASD, USA) which was set to a frame rate of 125 Hz at a resolution of 512 x 480 pixel. The camera shows a maximal sensitivity at ca. 630-660 nm. Ultra bright Light Emitting Diodes (LED) (HLMP-ED31-SV000, Agilent Technologies Inc., USA) composed the diffuse light source. The LEDs have their peak wavelength at λ_{peak} = 639 nm and a spectral halfwidth of $\Delta\lambda_{1/2}$ = 17 nm. A particular attention was paid to the illumination during the experiments. We checked its quasi-uniformity by illuminating evenly a white piece of paper.

We used a mixture of water and glycerin as an experimental fluid. A blue food color named Patent Blue V (Schumann und Sohn GmbH, Germany) was added to the fluid (maximum absorption at 638 nm in water at pH = 5).

2.2 Determination of the Particle-Wall Distance and Image Processing

The assessment of the correlation between the distance of a particle from the wall and the gray value of its image is the foundation for the separation of the particles within the illuminated layer. This correlation depends on the properties of the particles, on the absorption characteristics of the fluid, on the camera and on the illumination. The influence of the variations of the illumination or recording characteristics can be corrected with image processing. The correlation measurement has to be repeated each time the particles or the fluid change. This is made experimentally by displacing a cantilever with particles perpendicularly to the wall within a fluid with well-defined characteristics at well-defined steps. For each step one can note the gray value corresponding to the current particle-wall distance. It results in a graph representing the gray value of the particle images as a function of the distance from the wall. Figure 2 shows an example of such a graph.

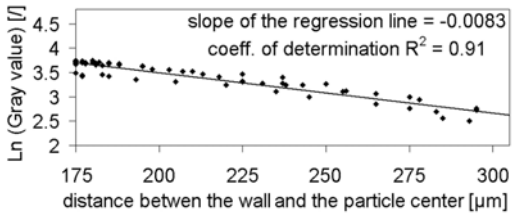

Fig. 2. Semi-logarithmic representation of the correlation between the average gray value of particle images and the distance of the particles from the wall.

For the separation of the wall flow, we defined classes of gray values. The number of classes and thus the number of sub-layers of particles depends on the penetration depth of the light into the model and on the size of the tracer particles themselves. The width of the gray value classes is different for each experiment, and is a compromise between the accuracy of the calculation and experimental uncertainty. The corresponding range of particle-wall distances is determined using the correlation presented above. Firstly we corrected background noise, camera noise and reflections on the illuminated surface. For this we identified the lowest intensity of each pixel in all of the source images, and stored it in a resulting file. This picture, called the minimum image, was then subtracted from each picture of the sequence. Following this, we separated the particle layers in the corrected pictures. The separation procedure was the same for each layer. A particle recognition process was implemented to identify all the pixels having their gray value within the chosen range and belonging to a particle, as well as all the pixels having a lower gray value but surrounding the selected central pixel. All the pixels which were not selected were marked and their new gray value was set to 0, i.e., they were reclassified as black. Thus, for each of the source images, there are as many resulting pictures as defined classes of gray values. For all the flow investigations presented in this paper, we only separated the two first sub-layers of particles closest to the wall. Figure 3 illustrates the particle discrimination process. On the left side of the picture one can see a detail of a source image after the correction. On the middle and on the right side there are the pictures resulting from the particle discrimination of two particles sub-layers. The pictures of Fig. 3 have been enlarged and artificially colored.

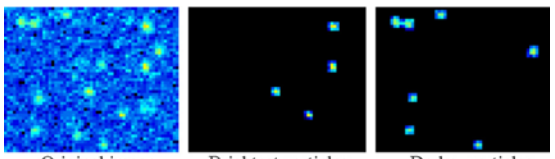

Fig. 3. Details of a corrected source image and results of the particle discrimination.

2.3 Calculation of the Velocity and Wall Shear Rate Fields

We calculated the motion of the particles in each separated layer by PIV using the commercial software DaVis 6 (LaVision GmbH, Germany). A standard PIV cross-correlation algorithm was used. No pre- or post-processing was done. Spurious vectors were filtered manually. In the case of an investigation at vaulted walls, the velocity values have to be corrected using either the surface function or a common projection technique. Maps of the flow streamlines and of the wall shear rate can be obtained based on the velocity fields.

3. Results

3.1 Steady Laminar Flow in a Straight Duct with a Rectangular Cross-Section

We first applied the new method to investigate the steady laminar flow at several low Reynolds numbers in a straight glass duct with a rectangular cross-section having the following dimensions: 5 x 50 x 200 mm^3. This is a well-understood reference test case and the analytical solution is known.

Here we present the results of the investigations at both Reynolds numbers Re = 1.1 and 5.5 ($Re = Ud/\nu$, with d = 5 mm the duct width, U the average velocity and ν the viscosity of the fluid) (see Table 1). Table 2 shows the details of the layer separation for each experiment, with the width of the defined classes of gray values, n, and the corresponding ranges of wall distances, d_{min} and d_{max}. For each value of d_{min} and d_{max}, we calculated the corresponding velocities v_{min} and v_{max} using the analytical solution. The point on the particles which were furthest from the wall, and had, therefore, the highest velocity, had a wall distance of 419 µm (wall distance to the particle surface + particle diameter) for the case A and of 508 µm for the case B. We assumed a linear progression of the velocity of a particle with its distance from the wall in a range of 510 µm and compared the velocities obtained in this way to the analytical solutions. The difference between both "real" and "linear" velocity was smaller than 10% between 0 µm and 510 µm. Thus the particles belonging to the separated layers were within the region where the velocity profile can be considered as linear. For the calculation of the velocity fields we used a cross correlation process with an interrogation window size of 128 x 128 pixel by a window overlap of 75%. We only considered the part of the surface where the effects of the side walls could be neglected, and calculated the average velocity over this area (case A: average of 169 vectors for the first layer and of 180 vectors for the second layer; case B: average of 97 vectors for the first layer and of 103 vectors for the second layer). The results are shown on Fig. 4.

Table 1. Characteristics of both flow investigations under steady laminar conditions.

	Re [/]	U [$mm \cdot s^{-1}$]	ν [$mm^2 \cdot s^{-1}$]	dye concentration [$mmol \cdot l^{-1}$]	d [µm]
case A	1.1	10.42	46.93	0.431	360
case B	5.5	11.96	10.96	0.259	350

Table 2. Width of the classes of gray values, corresponding wall distances and analytical solutions.

	Layer closest to the wall			Layer farther from the wall		
	n	d_{min}-d_{max} [µm]	v_{min}-v_{max} [$mm \cdot s^{-1}$]	n	d_{min}-d_{max} [µm]	v_{min}-v_{max} [$mm \cdot s^{-1}$]
case A	14	202-265	2.424-3.139	10	276-328	3.262-3.834
case B	10	192-221	2.651-3.033	8	229-244	3.137-3.332

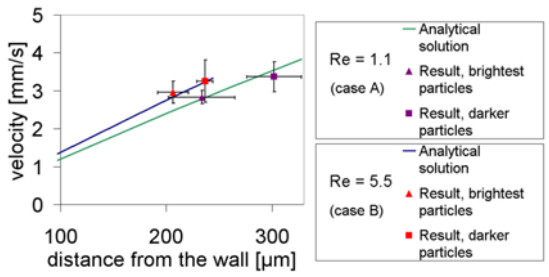

Fig. 4. Spatially averaged velocity versus distance from the wall, compared to the analytical solution, for both flow investigations. Errors bars are shown for the experimental results.

The measured near-wall velocities were in the velocity range which could be determined analytically. The differences between the analytical and experimental velocity values were smaller than 15%. Further flow investigations at several Reynolds numbers were performed. Their results confirmed the applicability of the method to obtain whole near-wall flow fields accurately.

3.2 Pulsatile Flow in a Straight Duct with a Rectangular Cross-Section

We then applied the new method to investigate the pulsatile flow in the straight duct presented in Sec. 3.1. The pulsatile flow was produced by superimposing an asymmetrical oscillation on a steady pressure-driven flow. The oscillation was created by a pulsatile pump. The flow pattern was measured with an ultrasonic transducer (Transonic Animal Research Flowmeter, Transonic Systems Inc., USA) and recorded using a computer with an Analog-to-Digital interface. Flow and image recording were triggered and synchronized.

Here we present the results of two cases with different frequencies. The flow parameters are the Womersley number α ($\alpha = a/2\sqrt{\omega/\nu}$, with a = 5 mm the duct width and ω the angular frequency of the waveform), the period T, the minimum and the maximum flow rates, and the maximum Reynolds number Re_{max} ($Re_{max} = aV/\nu$, with V the peak of the mean velocity) (see Table 3). First, the flow conditions were simulated by Computational Fluid Dynamics (CFD) to allow a comparison between experimental results and numerical solutions. The computation of the pulsatile flow was carried out with the FLUENT6 solver with an implicit time discretization scheme of a first order and a time step of 0.001 s. The flow curve obtained experimentally was interpolated by a cube spline function and imported by the flow solver. This function was set as an inlet boundary condition. Simulations were done with a second order upwind discretization scheme for the convective terms of the Navier-Stokes equations. During unsteady simulation the pressure-velocity correction method PISO was used. A no-slip boundary condition was set at all solid boundaries. The outflow was set to maintain a constant pressure. The numerical results were validated by a PIV investigation of the flow in the central plane of the model. Following this, the wall flow was investigated using the new method. Table 4 gives the details of the layer separation, i.e., the width of the classes of gray values, n, and the corresponding wall distances, $d_{min,exp}$ and $d_{max,exp}$. The wall distances chosen for the CFD results are shown on Fig. 5. The point on the particles which were furthest from the wall had a wall distance of 438 µm for the case C and of 464 µm for the case D. The CFD data show a linear progression of the velocity with the wall distance in this region. All the separated particles were thus in a layer, where the velocity can be considered as proportional to the wall distance. We used a cross correlation process with an interrogation window size of 128 x 128 pixel by a window overlap of 75% to obtain the whole velocity fields in each layer. We only considered the part of the surface where the effects of the side walls could be neglected. We calculated the average velocity over this area (about 30 vectors in each layer) and reported it as a function of time. The values were then averaged over three consecutive pulses. The upper part of Fig. 5 shows the velocities obtained experimentally for the case C as a function of time, compared to the velocities obtained by CFD. The comparison for the case D is shown on the bottom of the same figure.

Table 3. Characteristics of both flow investigations under pulsatile conditions.

	ν [$mm^2 \cdot s^{-1}$]	α [/]	T [s]	max. flow rate [$m^3 \cdot s^{-1}$]	min. flow rate [$m^3 \cdot s^{-1}$]	Re_{max} [/]	dye concentration [$mmol \cdot l^{-1}$]	d [µm]
case C	46.93	0.77	1.40	$2.57 \cdot 10^{-6}$	$-4.43 \cdot 10^{-6}$	1.9	0.431	360
case D	10.96	1.96	0.93	$10.25 \cdot 10^{-6}$	$-4.93 \cdot 10^{-6}$	18.7	0.259	350

Table 4. Width of the classes of gray values and corresponding wall distances.

	Layer closest to the wall		Layer farther from the wall	
	n	$d_{min,exp}$-$d_{max,exp}$ [µm]	n	$d_{min,exp}$-$d_{max,exp}$ [µm]
case C	14	197-227	10	229-258
case D	14	203-244	8	255-289

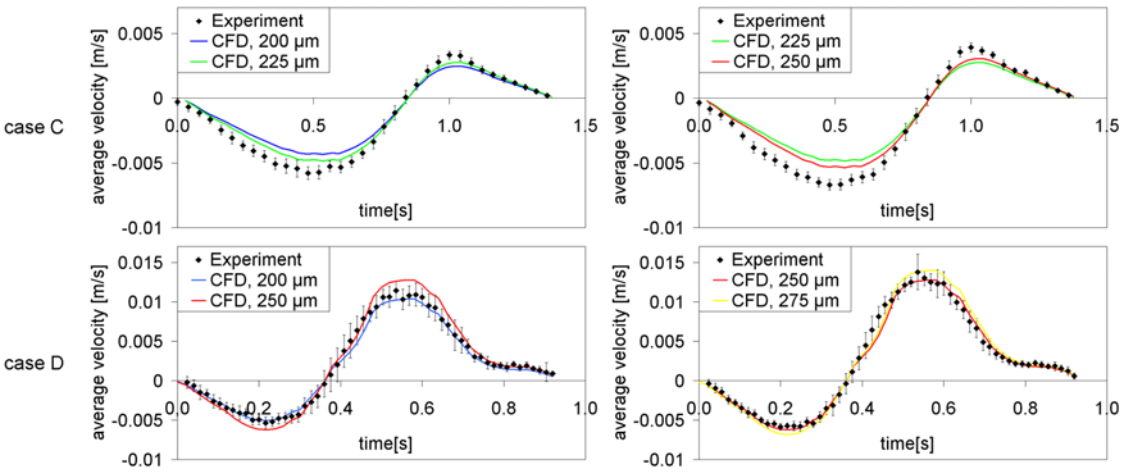

Fig. 5. Spatially averaged velocity versus time for the brightest (left) and the darker particles (right), compared to the CFD results, for both studied cases. Errors bars are shown for the experimental results.

The near-wall velocities measured with the new method are congruent with the numerical results obtained by CFD, even in the case of flow acceleration, deceleration or flow reversal. Another set of flow measurements was performed at several different frequencies, and from their results, we confirmed the applicability of the new method to investigate any type of pulsatile flow.

3.3 Steady, Laminar Flow in Two U-Shaped Ducts with a Backward Facing Step

We then studied the complex laminar steady flow in two different U shaped ducts with a backward facing step. The first duct had a rectangular, the second a nearly elliptical cross-section. In both cases, the flow is 3-dimensional, with separation and reattachment zones and curved streamlines.

Here we present the results of a flow investigation in the duct with vaulted walls at Re = 36 ($Re = a_c V/\nu$, with $\nu = 6.56 \cdot 10^{-6}$ $m^2 \cdot s^{-1}$, $V = 3.13$ $mm \cdot s^{-1}$ the average velocity and $a_c = 7.66$ mm the characteristic duct width). The geometry of the duct is shown in Fig. 6(a). The area of the cross-section before the step is $A_{1/2} = 260.68$ mm^2. The duct presents a curvature of 180 with a radius of 46 mm. After the step the cross-section A becomes nearly elliptical and twice as large. First, the flow was calculated by CFD using the Fluent6 solver. The inflow condition was the velocity inlet V with a plug flow profile. The pressure-velocity correction method SIMPLEC was used to improve the convergence of solution in case of complicated flow patterns including recirculations. A no-slip boundary condition was set at all solid boundaries. The outflow was set to maintain a constant pressure. The validity of the CFD model was confirmed by a PIV investigation in the central plane of the model. We then applied the new method to investigate the wall flow immediately after the step.

The class of gray values for the layer closest to the wall had a width of 14. On the correlation diagram related to this experiment, this corresponds to a range of wall distances between 175 and 230 μm. For the second layer we had a range of 6 gray values. The results therefore show a range of wall distances between 230 and 270 μm. The point on the particles which was furthest from the wall had in this case a wall distance of 445 μm. In this region, the CFD data show a linear progression of the velocity with the wall distance. Figure 6 (b) shows the so-called max-min image of the flow. This image is the result of the calculation of the difference between the maximum and the minimum image. The minimum image has already been explained in Sec. 2.2. The maximum image is obtained in the same way: one searches for the maximum instead of for the minimum intensity of each pixel. Thus the max-min file shows the particles' trajectories, because the particles which are moving between two time steps are the brightest objects in the picture. This picture is very useful to observe the flow structures qualitatively, especially near the reattachment line. For the velocity calculation we used an adaptive cross-correlation process with a final interrogation window size of 32 x 32 pixel with an overlap of 42%. The true value of the velocity was obtained by transforming the measured displacement vectors into the tangential velocity vectors and calculating the resulting vector length. For both layers we averaged 18 consecutive vector fields. Figure 7 shows a comparison between the projections of the velocities in the X-Y plane obtained experimentally for the first layer and by CFD at a wall distance of 200 μm. Figure 8 shows the wall shear rate distribution for the same layer. We divided the corrected length of the vector with the mean wall distance (200 μm). We also compared the velocity profiles along several Y-positions. Figure 9 shows the comparison at the Y-position shown on Fig. 7 for both layers.

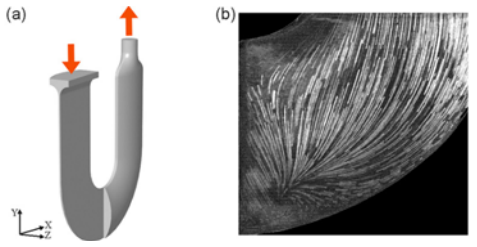

Fig. 6. (a) Geometry of the nearly elliptical U shaped duct with a backward facing step. (b) Max-min picture showing the trajectories of the particles at Re = 36.

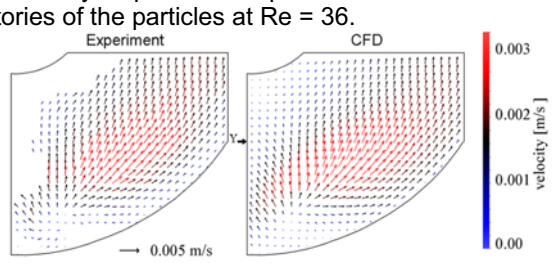

Fig. 7. Projections of the time-averaged velocities in the X-Y plane obtained experimentally for the brightest particles (left) and by CFD for a wall distance of 200 μm (right) at Re = 36.

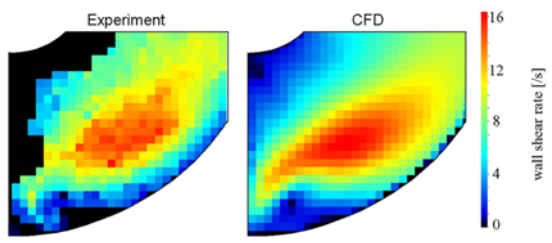

Fig. 8. Time-averaged wall shear rate fields obtained experimentally for the brightest particles (left) and by CFD for a wall distance of 200 μm (right) at Re = 36.

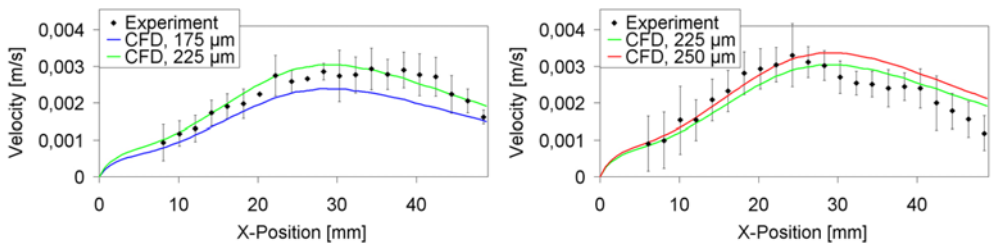

Fig. 9. Comparison of the velocity along a Y-position (shown on Fig. 7) obtained for the brightest (left) and the darker (right) particles and by CFD at Re = 36. Error bars are shown for the experimental results.

The experimental results concord with the numerical simulation. Not only the velocities but also the values of the wall shear rate are congruent. For this parameter the differences between the numerical and the experimental values are smaller than 15%. It was possible to repeat the experiments at several Reynolds Numbers successfully (Re = 36…46).

4. Discussion

The first experimental results obtained with the new method presented in this paper concur well with analytical or numerical solutions. Before continuing to develop the technique, we have to quantify the measurement error. The most likely error sources are the particles' behavior and the determination of their distance from the wall.

All the experiments described above were based on the assumption that the particles follow the flow, even in a region very close to the wall. As the method works well, this assumption was validated for the first development step. Further theoretical and experimental studies are now necessary to determine the particles' behavior, especially near the wall. Investigating the lift forces and the particle-wall interaction should provide precious information about the measurement error. Moreover, we already know that the measurement accuracy can be improved:

- By reducing the particle size. Smaller particles would follow the flow better. Since the particle image diameter would probably be smaller, this would optimize the PIV calculation (Hu et al., 1998). It would be possible to increase the number of particles and thus their image density by keeping the same volume fraction. This could improve the PIV calculation and/or the spatial resolution.
- By refining the measurement of the correlation between the gray value and the distance from the wall, and by improving the picture correction to get less noisy images.
- By reducing the width of the classes of gray values and improving the separation procedure of the particle layers in order to optimize the PIV calculation and to reduce the RMS-values.

5. Conclusion

This paper deals with the preliminary evaluation of a newly developed method designed to assess the shear flow at vaulted walls with spatial and temporal resolution. Initially this method was used to investigate the flow in a straight duct under steady laminar (Re = 1.1 and 5.5) and pulsatile conditions (α = 0.77 and 1.96). The experimental results showed a deviation from the analytical or the numerical solutions of less than 20%. Then the steady laminar flow (Re = 36) in a U-shaped duct with vaulted walls and a sudden expansion was assessed. Again the experimental results agreed well with the numerical solutions.

Therefore, we can conclude that the new method presented above is of value to investigate the shear flow at planar as well as at curved or even vaulted walls, in simple as well as in complex models, and under steady as well as under pulsatile flow conditions. Further investigations and theoretical studies are necessary to assess the measurement error. Technical improvements are possible in order to increase the measurement accuracy.

References

Asakura T. and Karino T., Flow patterns and spatial distribution of atherosclerotic lesions in human coronary arteries, Circ. Res., 66 (1990), 1045-1066.

Asztalos B., Yamane T., Nishida M., Masuzawa T. and Konishi Y., Evaluation of shear and recirculation in centrifugal artificial heart by flow visualization, J Visualization, 3-1 (2000), 79-92.

Heinzen Ch., Herstellung von monodispersen Mikrokugeln durch Hydroprilling, (1996), Eidgenössische Techn. Hochschule, Zürich.

Hu H., Saga T., Kobayashi T., Okamoto K. and Taniguchi N., Evaluation of the cross correlation method by using PIV Standard Images, J Visualization, 1 (1998), 87-94.

Kroll M. H., Hellums J. D., McIntire L. V., Schafer A. I. and Moake J. L., Platelets and shear stress, Blood, 88-5 (1996), 1525-1541.

Nerem, R. M., Alexander, R. W., Chappell D. C., Medford R. M., Varner S. E. and Taylor W. R., The study of the influence of flow on vascular endothelial biology, Am J Med Sci, 316-3 (1998), 169-175.

Morton W. and Cumming R., A technique for the elucidation of Virchow's triad, Ann NY Acad Sci, 283 (1977), 477.

Author Profile

Perrine Debaene: She received her Diploma in Biomedical Engineering - Biomechanics/Biomaterials from the Technological University of Compiègne, France, in 2001. She wrote her diploma thesis at the Biofluidmechanics Laboratory, Charite Berlin, about the flow visualization in a blood pump of a ventricular assist device. Perrine Debaene has worked as a research assistant in this laboratory since 2001. She defended her Ph.D. thesis, which was supported by the German National Academic Foundation, in April 2005. Her research interests are quantitative visualization, PIV, flow in natural and artificial organs and biomechanics.

Ulrich Kertzscher: He received his diploma in Physical Engineering from the Technical University Berlin in 1989, and his doctorate (Eng.) from the Technical University Karlsruhe in 1994. Since 1997 Ulrich Kertzscher works at the Biofluidmechanics Laboratory, Charite Berlin, as a research assistant. His research interests are quantitative visualization, PIV, flow optimization of the artificial organs and analysis of the blood flow in the native vessels.

Leonid Goubergrits: He received his MSc (Physics) in Fluid Mechanics in 1993 from the Moscow Institute of Physics and Technology, Department of Aeromechanics and Flying Machines. He also received his doctorate in Engineering in 2000 from the Technical University of Berlin. Since 1996, Leonid Goubergrits works at the Biofluidmechanics Laboratory, Charite Berlin, as a research assistant. His research interests are Quantitative Visualization, PIV, CFD, flow optimization of the artificial organs and analysis of the blood flow in the native vessels.

Klaus Affeld: He received his diploma degree in Aircraft Engineering in 1962 and his doctorate (Eng.) in fluid mechanics in 1969 from the Technical University Berlin. He worked at the institute of aircraft engineering in Berlin before starting his doctorate. After obtaining his doctorate, he worked as a researcher in Biofluidmechanics in the development of an artificial heart and taught Biofluidmechanics at the Technical University Berlin. In 1987, he founded the Biofluidmechanics Laboratory within the Charite. His research interests are blood flow including flow in artificial organs, experimental methods in fluid mechanics, biomedical engineering and biomechanics.